CHAPTER-5

STUDIES ON $Bi_{12}TiO_{20}$ CERAMIC

5. Introduction

The several mixed metal oxides such as TiO_6, NbO_6 or TaO_6 octahedral units, such as $SrTiO_3$[1], $BaTi_4O_9$[2], $K_4Nb_6O_{17}$[3], $InTaO_4$[4], and $In_{1-x}Ni_xTaO_4$[5], had been extensively studied in past decades not only as photocatalysts in the field of water splitting but also these metal oxides showed their electronic device applications. In present time environmental blow up has become one of the most salient topics in photo-catalysis where $TiO_2$is the most efficient photocatalyst for the disgrace of organic pollutant but the obstacle that $TiO_2$is efficient only in UV radiation(λ<360 nm).When the sunlight is contain of less than 2% ultraviolet light, so it was important to develop new photo-catalyst. Sillenite materials are of great importance because of their photorefractive, piezoelectric, electrooptic, and photoconductive properties [6–8]. Newly, the bismuth titanate family with different layered perovskite compounds such as sillenite $Bi_{12}TiO_{20}$, pyrochlore $Bi_2Ti_2O_7$ and Aurivillius-type $Bi_4Ti_3O_{12}$, has been greatly concerned as a class of novel and promising photocatalysts with useful application in electronic device[9]. The bismuth titanateis generally synthesized by the solid state reaction [10], chemical solution decomposition [11][11], hydrothermal[12] [12] or solvothermal method [13][13]. Among them, $Bi_{12}TiO_{20}$ is an important crystal belongs to sillenite compound with all embracing formula $Bi_{12}TiO_{20}$. It's crystals structure is formed by polyhedron network connects to the geometrically regular TiO_4tetrahedra.Each of the tetrahedra is formed by four oxygen anions while the Ti cation occupies the tetrahedral interstice[5]. The various

morphological structure of $Bi_{12}TiO_{20}$ such as nano-spheres, nano-wires and micro flowers has been synthesized through a hydrothermal process [14–18].

In the present work, $Bi_{12}TiO_{20}$ polycrystalline material was successfully synthesized by chemical route. This present route is different from other chemical route where an alkoxide, oxynitrate, or chloride of titanium is used as titanium source; which very expensive materials. In the present route, the cheap raw material, solid TiO_2, is used and other metal ions were taken in solution form. The advantage of this route to form the nanocrystalline BTO powder because of the mixing process is performed in a solution of metal nitrate along with cheap TiO_2. The present synthesis method is the simplest synthesis technique to get BTO nanocrystalline powder in comparison to other synthetic methods as listed in table 1. The obtained $Bi_{12}TiO_{20}$ polycrystalline by this route were characterized by XRD, SEM, EDX, and TEM, along with first time dielectric and electrical studies.

5 .1 Experimental details

a *Material Synthesis*

$Bi_{12}TiO_{20}$ was synthesized by the chemical route using analytical grade chemicals, Bi $(NO_3)_2$. $6H_2O$ (99% Merck, India) and TiO_2 (99% Merck, India) as starting materials. The stoichiometric amount of bismuth nitrates was dissolved in de-ionized distilled water along with appropriate amount of citric acid ($C_6H_8O_7$ .H_2O, 99% Merck, India) as equivalent to the metal ions. Stoichiometric amount of solid $TiO_2$was added in the solution. The resulting mixture was heated on a hot plate magnetic stirrer at 70 – 80 °C to evaporate excesses water. On ignition, a fluffy mass obtained which burns with a sooty flame. The obtained fluffy mass was crushed into

fine powder with the help of mortar and pestle. The resultant dry powder was calcined at 600 °C for 6 h in the electrical muffle furnace and made pellets (13.0 mm diameters, 1.6 mm thicknesses) using 2 wt% polyvinyl alcohol (PVA) as a binder. These pellets were sintered at 800 °C for 6 hand further used for different physiochemical characterizations such as XRD, SEM, TEM, EDX, and AFM.

b. *Characterization*

The crystalline phase of sintered BTO ceramic was identified by X-ray diffraction analysis (Rigakuminiflex 600, Japan) employing Cu-Kα radiation (λ = 1.54 Å). The microstructure and elemental analysis of the BTO were observed by scanning electron microscope (ZEISS, model EVO–18 research; Germany) energy-dispersive X-ray spectroscopy, EDX (Oxford instrument; USA), respectively. Transmission electron microscope (TEM, FEI TECANI G^2 20 TWIN; USA) was used for particle size determination. The surface morphology was examined by atomic force microscopy (NTEGRA Prima, Germany). The frequency and temperature dependence dielectric of silver coated pellets were carried out using LCR meter (PSM 1735, NumetriQ 4^{th} Ltd. U.K.).

5.3 Results and discussion

5.3.1 Microstructural studies

X-ray patterns were indexed and well matched with the $Bi_{12}TiO_{20}$ peaks and shows good agreement with the single phase of silleniteBi$_{12}$TiO$_{20}$structure reported in JCPDS file number 34-0097, which confirmed the formation of $Bi_{12}TiO_{20}$ phase in sintered as well as calcined powder. As expected, the pure $Bi_{12}TiO_{20}$ phase can only be obtained when the amounts of bismuth and titanium are very close to the

stoichiometric ratio. It was observed that in the sintering process no major changes in crystalline phase intensity occurred. There is no evidence for the presence of a secondary phase in the ceramic.

XRD patterns of $Bi_{12}TiO_{20}$calcined at 600 ºC and sintered at 800 ºC for 6h are shown in Fig.5.1

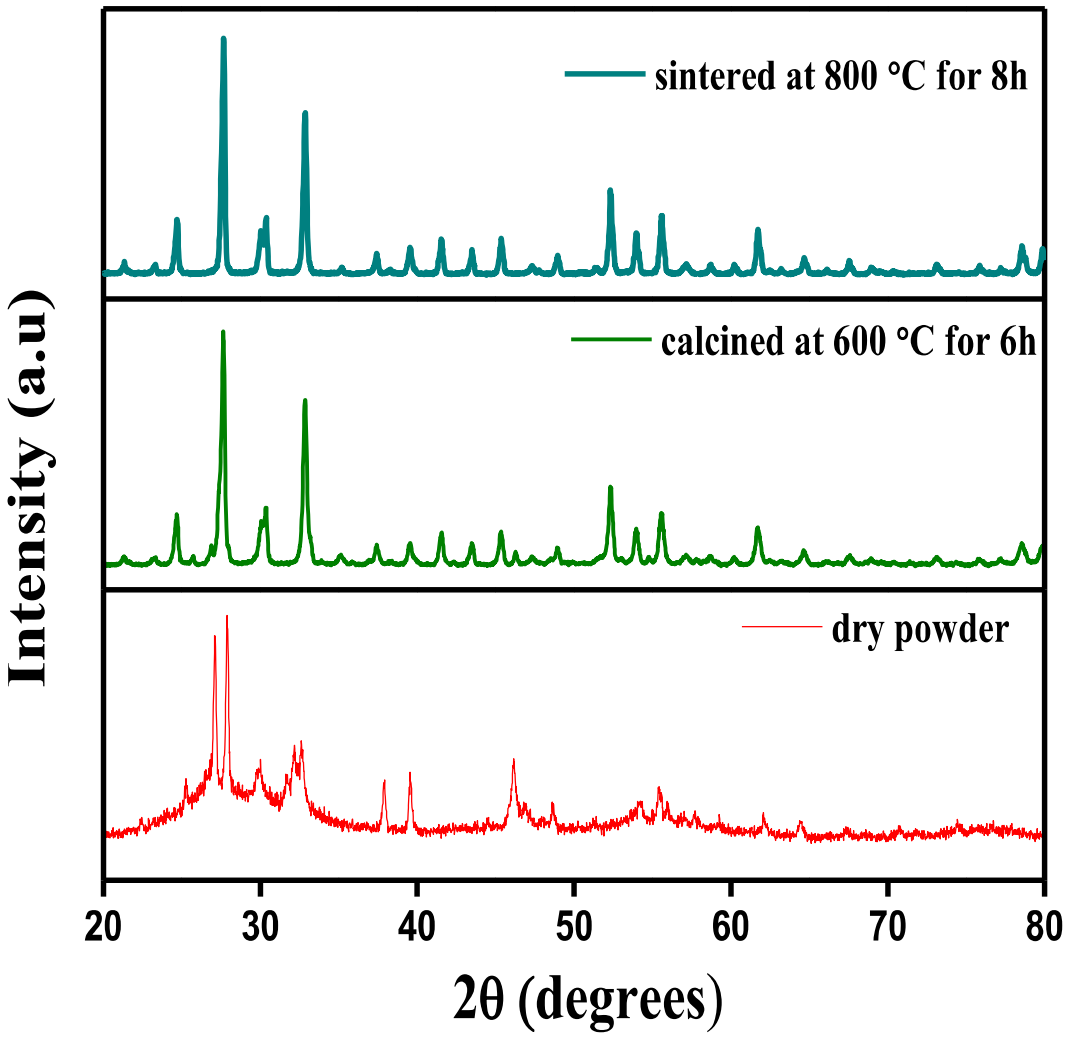

Fig. 5.1 XRD patterns of $Bi_{12}TiO_{20}$ (BTO) ceramic (a) calcined at 600 ºC (b) sintered at 800 ºC for 6 h, respectively.

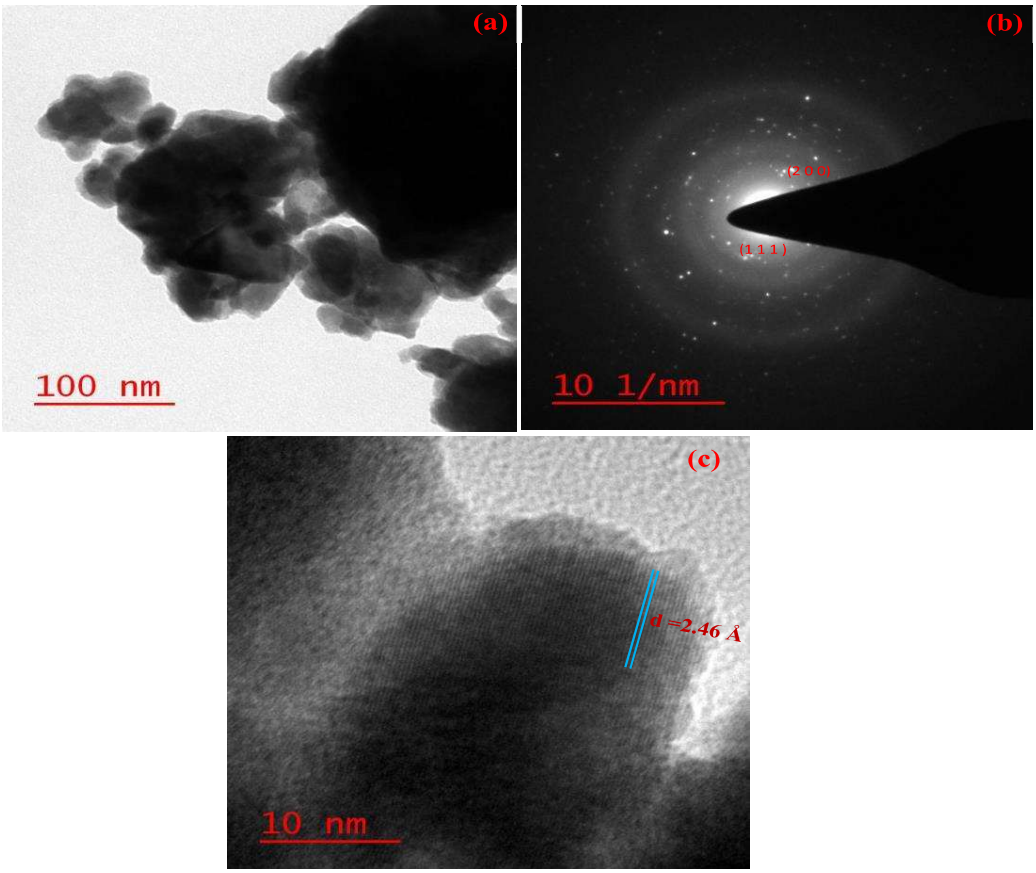

Fig. 5.2(a) Bright field TEM image (b) Selected area diffraction (SAED) pattern (c) HR-TEM image of BTO ceramic.

A representative bright field TEM image and selected area electron diffraction patterns (SAED) of the $Bi_{12}TiO_{20}$sintered at 800 ºC for 6 h are shown in Fig. 2(a-b). It is clearly displayed from the TEM image of $Bi_{12}TiO_{20}$that the ceramic fabricated by this route is nano-crystalline in nature. The particle size of the $Bi_{12}TiO_{20}$ was found to be in the range of 60±10 nm. Fig. 2(b) displayed the SAED patterns of the $Bi_{12}TiO_{20}$ceramic sintered at 800 ºC for 6 h. The diffraction patterns have been indexed on the basis of cubic crystal structure. The inter-planar spacing (d_{hkl}) measured from the SAED are in agreement with the values obtained from XRD data

(JCPDS card No. 34-0097)which confirmed the presence of single-phase crystalline material.

The additional spots observed in the SAED patterns are from adjacent grains and sub-grains due to their orientation in different directions. Fig. 2(c) presents the HR-TEM lattice fringes of the synthesized $Bi_{12}TiO_{20}$, which clearly revealed the well-defined lattice fringe confirming the high crystallinity and absence of phase separation of the material. The measured crystal lattice fringe d-spacing of $Bi_{12}TiO_{20}$ was approximately 2.46 Å corresponding to the (321) plane, which shows a good agreement with the XRD results as shown in Fig. 1b.

Fig. 3 (a) presents a SEM image of the fractured surface of the $Bi_{12}TiO_{20}$ sintered at 800 ºC for 6 h. The $Bi_{12}TiO_{20}$ ceramic exhibited a bimodal grain size distribution with small grains, approximately 0.6 μm in diameter, and large grains, approximately 3.7 μm in size.

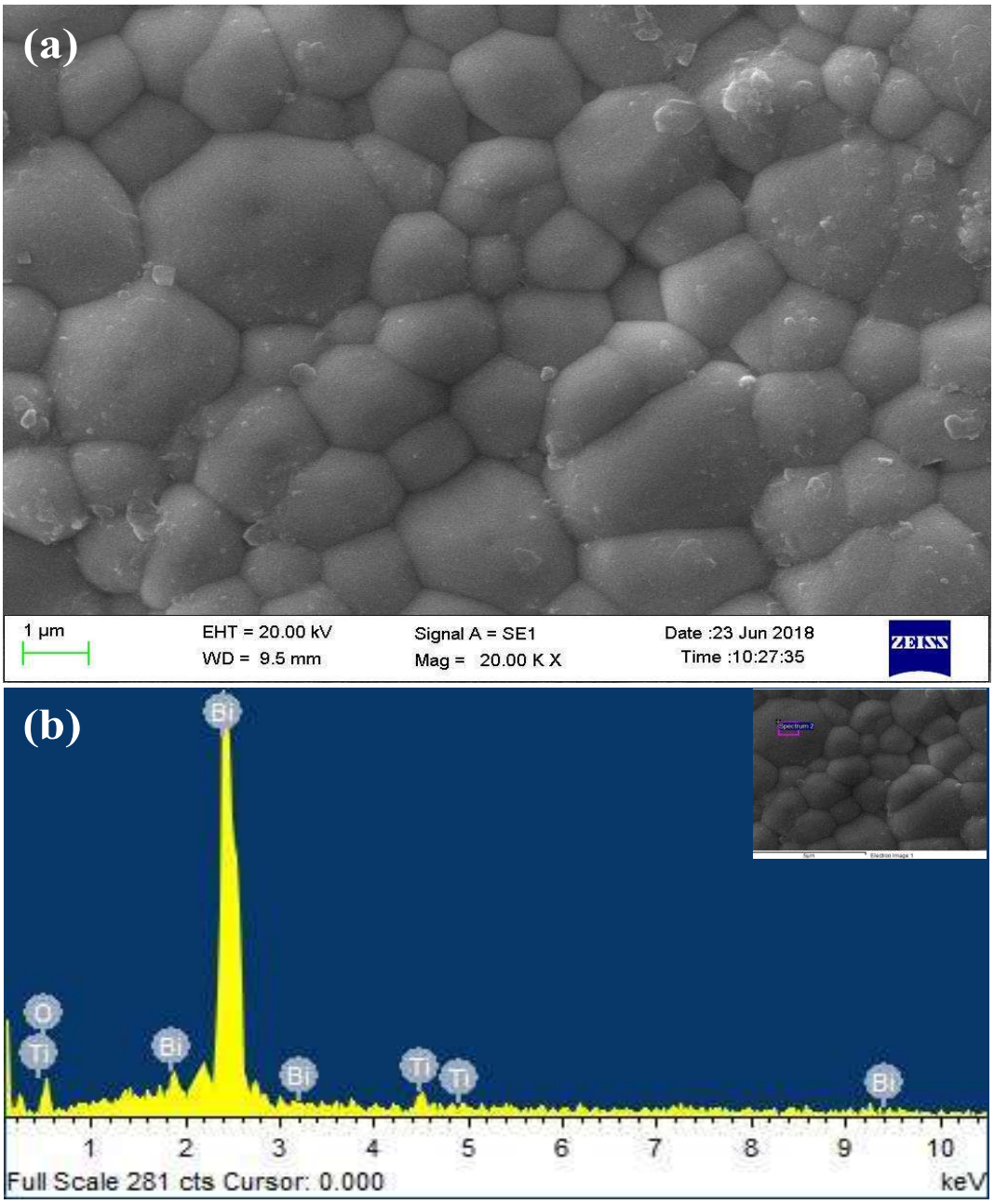

Fig.5. 3(a)SEM image of the fractured surface (b) EDX spectra of BTO ceramic sintered at 800 ºC for 6 h

The bimodal nature morphology of the grains in the SEM image is similar to results reported elsewhere [19]. Fig. 3 (b) presents the energy dispersive X-ray analysis (EDX) spectrum of the $Bi_{12}TiO_{20}$ ceramic collected during the SEM observations. The spectrum revealed the presence Bi, Ti, and O in the stoichiometric

ratio of $Bi_{12}TiO_{20}$ceramic. The spectrum showed no impurity elemental peaks. The atomic percentage of Bi, Ti, and O ions obtained from the EDX data were38.46, 3.28and 67.25, respectively, which is in accordance with the expected stoichiometry of the $Bi_{12}TiO_{20}$.

Fig. 4displayed the different view of AFM images (a) 2D for grain boundaries (b) 3D for surface roughness and (c) histogram graph for particle size distribution of sintered BTO ceramic.

Figure 4(a) displayed the clear grain boundaries with a comparable grain size of the $Bi_{12}TiO_{20}$ ceramic. The average roughness (R_a) and root mean square (R_q) data are obtained as 57. 82 nm and 72.35 nm, respectively on scanned area 11 mm× 11 mm. The distribution of particles on the surface is also recorded by the three dimensional image as shown in Fig. 4(b). The maximum peak-valley depth (R_v), maximum profile peak height (R_p) and maximum height of the profile (R_{max}) of three-dimensional structures are found to be 207.28, 155.72, 362.99 nm, respectively. Figure 4(c) reveals the histogram of grain size indicates the most of the grain are in size range of 0.5-1.0 μm and the average grain size obtained by this plots are found to be 0.75 μm , which substantiate with SEM image result of $Bi_{12}TiO_{20}$ as mentioned earlier in Fig. 3.

5.3.2. Dielectric behavior

Fig. 5.3 (a, b) displayed the temperature dependence of the dielectric constant (ε') and dielectric loss (tan δ) at a few representative frequencies.

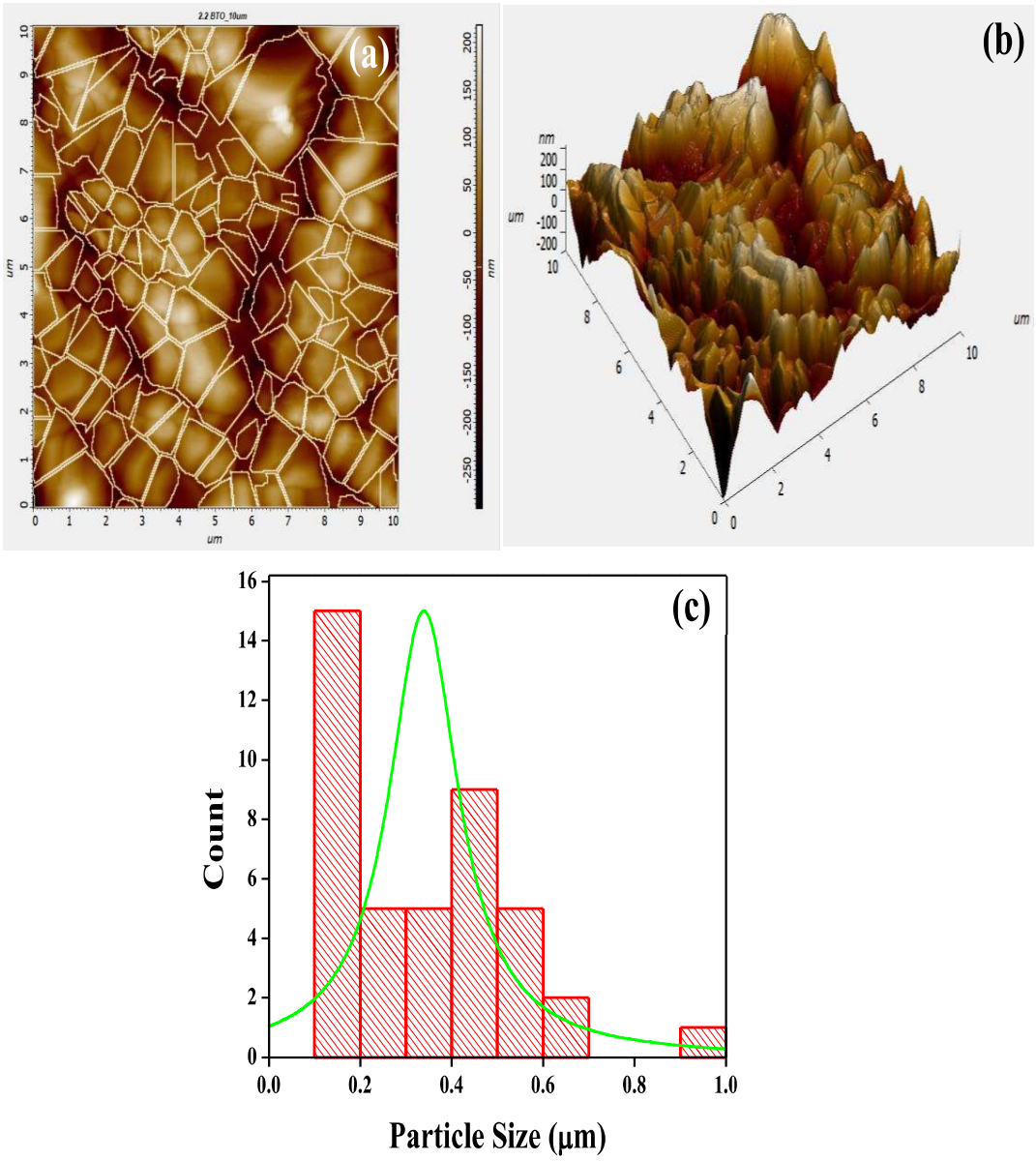

Fig.5.4. AFM images (a) 2D for grain boundaries (b) 3D for surface roughness and (c) histogram graph for particle size distribution of sintered BTO ceramic.

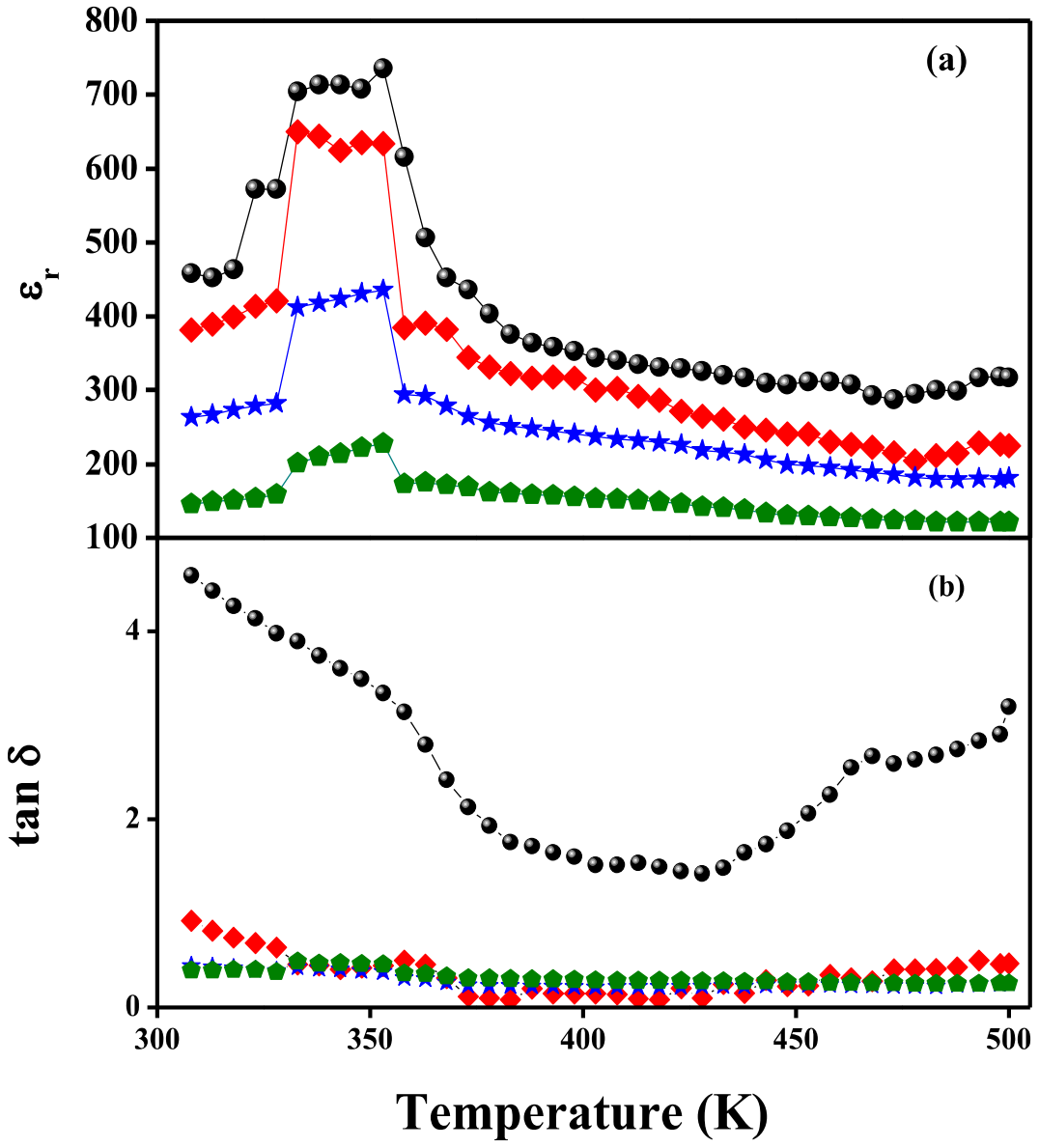

Fig. 5.5 Temperature dependence (a) dielectric constant (ε'), (b) dielectric loss (tan δ) at a few representative frequencies.

Fig. 5.5 shows that in the temperature range, 350–500 K, both the dielectric constant and loss values shows the weak temperature-dependent behavior. However, below 350 K, the dielectric constant (ε') and dielectric loss (tan δ) increased continuously with increasing temperature, but the rate of these accession was not the same. The stinging increase in the ε' value was associated to space charge polarization and the

chemical micro-heterogeneities present in these ceramics[20]. It is observed that temperature has a large impact on the dielectric properties of $Bi_{12}TiO_{20}$. In addition, at any given temperature, the dielectric constant and dielectric loss decreases with increasing in frequency, and the dependence of dielectric properties with increasing frequency varies with temperature.

Fig. 6 (a-b) displayed the variation of the real dielectric constant (ε'), and dielectric loss (tan δ) as a function of frequency, at few selected temperatures 308, 348, 388, 428 and 468 K. In the fig. 6 (a) towards low frequency region, a dielectric constant plateau was followed by a relaxation step.

The high dielectric constant at low frequency was contributed to interfacial polarization which may be arises due the heterogeneous microstructure of $Bi_{12}TiO_{20}$and similar type perovskite which consists of conducting or semi-conducting grains with insulating grain boundaries[21,22]. At higher frequencies, the space charges weakly follow the varying AC field and hence a relaxation step is observed with decreasing in dielectric constant [23].Fig. 6 (b) display that the dielectric loss of the $Bi_{12}TiO_{20}$ ceramic was found to be higher at low frequencies, up to 10^3 Hz as exceptional behavior at 308 K, and then almost remains constant from the high frequency range of 10^3–10^7 Hz. This shows that dielectric loss decreases intensely with increasing frequency. In addition, the dielectric loss increases with increasing temperature in the measured temperature range. The frequency and temperature effect on the dielectric loss highlights the interfacial polarization of the grain boundaries within the ceramic in the low frequency region.

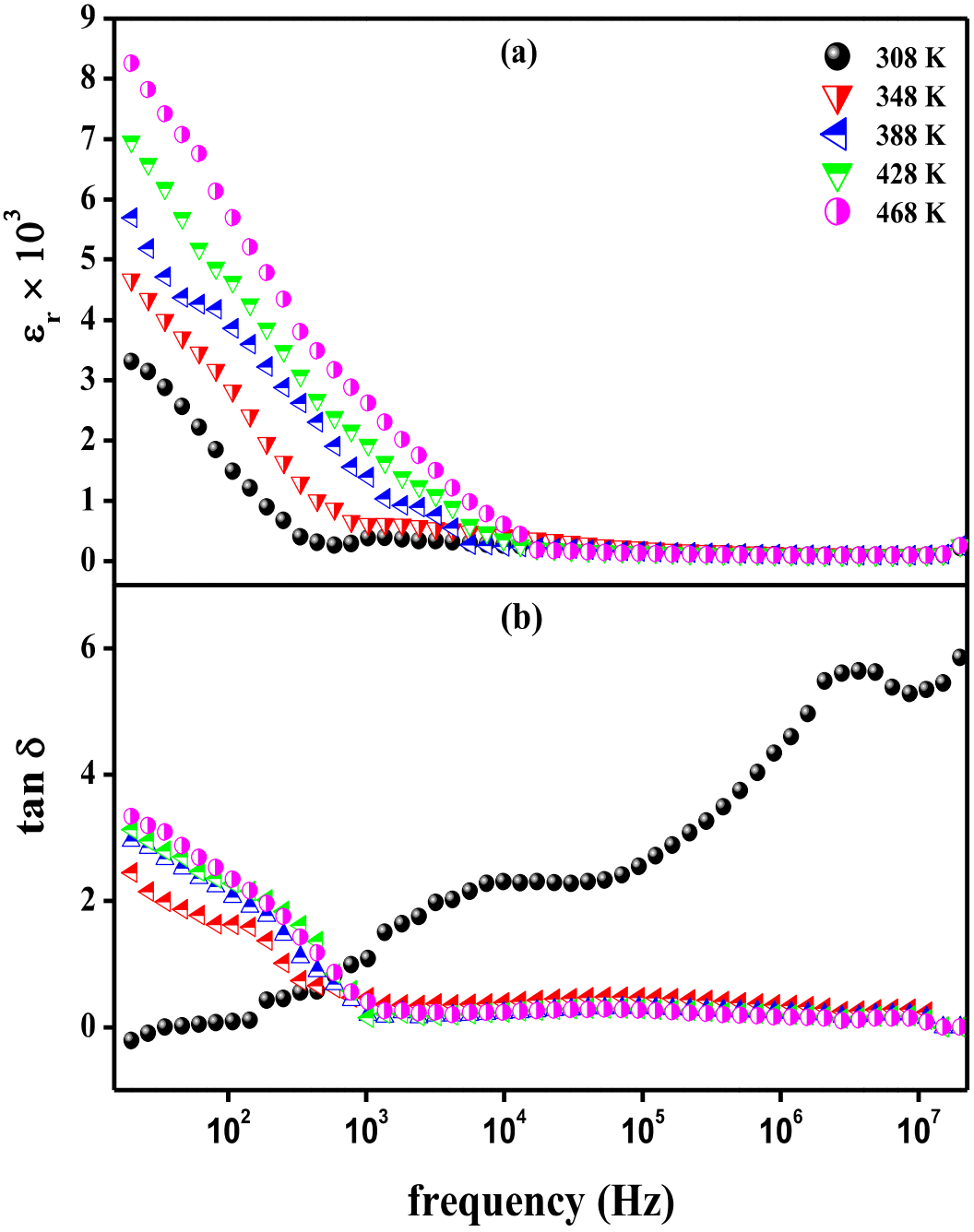

Fig.5.6 Variation of (a) real dielectric constant (ε'), (b) dielectric loss (tan δ) as a function of frequency at few selected temperatures

5.4 Conclusions

Single-phase of $Bi_{12}TiO_{20}$ nanocrystalline ceramic powders with an average particle size found in the range of 50±20nm has been fabricated at a relatively low temperature with a short calcination temperature at 600 °C for 6 h than other reports by using chemical routes along with inexpensive and stable solid TiO_2 powder as the titanium source. XRD and EDX studies confirmed the purity and stoichiometry of the $Bi_{12}TiO_{20}$ ceramic. The best $Bi_{12}TiO_{20}$ ceramic exhibited a high dielectric constant (6.1×10^3) with low dielectric loss (2.45) at 100 Hz. These results show that the dielectric properties of $Bi_{12}TiO_{20}$ ceramic are dependent upon the methodology of synthesis.

References:

[1] Thanabodeekij N, Gulari E, Wongkasemjit S. Bi12TiO20 synthesized directly from bismuth (III) nitrate pentahydrate and titanium glycolate and its activity. Powder Technology. 2005;160:203–208.

[2] Liu Y, Guo H, Zhang Y, et al. Heterogeneous activation of peroxymonosulfate by sillenite Bi25FeO40: Singlet oxygen generation and degradation for aquatic levofloxacin. Chemical Engineering Journal [Internet]. 2018;343:128–137. Available from: https://doi.org/10.1016/j.cej.2018.02.125.

[3] Zhang Y, Jiang Z, Huang J, et al. Erratum: Titanate and titania nanostructured materials for environmental and energy applications: a review (RSC Adv. (2015) 5 (79479-79510)). RSC Advances [Internet]. 2015;5:82632. Available from: http://dx.doi.org/10.1039/C5RA90088C.

[4] Wiehl L, Friedrich A, Haussühl E, et al. Structural compression and vibrational properties of Bi 12SiO20 sillenite from experiment and theory. Journal of Physics Condensed Matter. 2010;22.

[5] Roon V, Leeuw D, Breakdown SW, et al. Direct splitting of water under visible light irradiation with an oxide semiconductor photocatalyst. 2002;704:2000–2002.

[6] Peltier M, Micheron F, Currents TS. Volume hologram recording and charge transfer process in Bi12SiO20 and Bi12GeO20. 1996;3683.

[7] Venturini EL, Spencer EG, Ballman AA. ElastoOptic Properties of Bi12GeO20 , Bi12SiO20 , and Sr x Ba1 − x Nb2O6. 2013;1622:4–7.

[8] Chmyrev VI, Skorikov VM, Larina E V. Doping Effect on the Optical , Electro-optic , and Photoconductive Properties of Bi 12 MO 20 (M = Ge , Si , Ti). 2006;42:381–392.

[9] Sun X, Bao T, Sun L, et al. Comparative study on the performance of new highly visible-light responsive photocatalyst Bi20TiO32 with P-25. Advanced

Materials Research. 2011;146–147:1540–1543.

[10] Kong LB, Ma J, Zhu W, et al. Preparation of Bi 4 Ti 3 O 12 ceramics via a high-energy ball milling process. 2001;108–114.

[11] Feng W, Hong X, Wang H, et al. Photocatalytic property of perovskite bismuth titanate. 2004;52:109–116.

[12] Pei LZ, Liu HD, Lin N, et al. Bismuth titanate nanorods and their visible light photocatalytic properties. 2015;622:254–261.

[13] Ren J, Liu G, Wang Y, et al. A novel method for the preparation of Bi 2 Ti 2 O 7 pyrochlore. Materials Letters [Internet]. 2012;76:184–186. Available from: http://dx.doi.org/10.1016/j.matlet.2012.02.073.

[14] Hou J, Qu Y, Krsmanovic D, et al. Hierarchical assemblies of bismuth titanate complex architectures and their visible-light photocatalytic activities †. 2010;2418–2423.

[15] Li JF, Wang K, Zhu FY, et al. (K, Na) NbO3-based lead-free piezoceramics: Fundamental aspects, processing technologies, and remaining challenges. Journal of the American Ceramic Society. 2013;96:3677–3696.

[16] Yao WF, Wang H, Xu XH, et al. Characterization and photocatalytic properties of Ba doped Bi 12 TiO 20. 2003;202:305–311.

[17] Zhang Y, Zhang Y, Fu B. Effects of pH on the crystal structure , morphology and microwave dielectric properties of Bi 12 TiO 20 ceramics synthesized by citrate sol – gel method. 2015;3179–3185.

[18] Nogueira AE, Longo E, Leite ER, et al. Visible-light photocatalysis with bismuth titanate (Bi 12 TiO 20) particles synthesized by the oxidant peroxide method (OPM). Ceramics International [Internet]. 2015;41:12073–12080. Available from: http://dx.doi.org/10.1016/j.ceramint.2015.06.024.

[19] Pandirengan T, Arumugam M, Durairaj M. Development of high dielectric dual phase [Bi4Ti3O12]X–[CaCu3Ti4O12]1 − X nanocomposite thin films for

modern microelectronic device applications. Thin Solid Films [Internet]. 2017;628:117–126. Available from: http://dx.doi.org/10.1016/j.tsf.2017.03.021.

[20] Singh L, Kim IW, Sin BC, et al. Combustion synthesis of nano-crystalline Bi2/3Cu3Ti2.90Fe0.10O12 using inexpensive TiO2 raw material and its dielectric characterization. Powder Technology [Internet]. 2015;280:256–265. Available from: http://dx.doi.org/10.1016/j.powtec.2015.04.025.

[21] Singh L, Kim IW, Sin BC, et al. Study of dielectric, AC-impedance, modulus properties of 0.5Bi0.5Na0.5TiO3·0.5CaCu3Ti4O12 nano-composite synthesized by a modified solid state method. Materials Science in Semiconductor Processing [Internet]. 2015;31:386–396. Available from: http://dx.doi.org/10.1016/j.mssp.2014.12.025.

[22] Kumar A, Yadava SS, Gautam P, et al. Magnetic and dielectric studies of barium hexaferrite (BaFe 12 O 19) ceramic synthesized by chemical route. Journal of Electroceramics. 2019;42:47–56.

[23] Amow G, Au J, Davidson I. Synthesis and characterization of La4Ni3-xCoxO10±δ ($0.0 \leq x \leq 3.0$, $\Delta x = 0.2$) for solid oxide fuel cell cathodes. Solid State Ionics. 2006;177:1837–1841.